INTERNATIONAL JOURNAL OF CLIMATOLOGY, VOL. 15, 613–623 (1995) 551.524.33:551.526.6(26):530.1

UNIVERSAL SPECTRUM FOR INTERANNUAL VARIABILITY IN *COADS* GLOBAL AIR AND SEA-SURFACE TEMPERATURES

A. MARY SELVAM AND R. R. JOSHI
Indian Institute of Tropical Meteorology, Pune 411 008, India

Received 7 January 1994
Accepted 15 September 1994

ABSTRACT

Continuous periodogram spectral analyses of 28 years (1961–1988) of seasonal (September–November) mean COADS global surface (air and sea) temperature time-series show that the power spectra follow the universal inverse power law form of the statistical normal distribution. An inverse power law form for power spectra of temporal fluctuations implies long-range temporal correlation and is a signature of self-organized criticality. Universal quantification for self-organized criticality presented in this paper is consistent with a recently developed cell dynamical system model for atmospheric flows, which predicts such non-local connections as intrinsic to quantum-like mechanics governing flow dynamics. The universal spectrum for interannual variabiality rules out linear secular trends in global surface (air and sea) temperatures.

KEY WORDS: self-organized criticality; Comprehensive Ocean Data Set; sea-surface temperature; air temperature; chaos fractal; interannual variability in surface temperature

INTRODUCTION

Surface (air and sea) temperatures exhibit interannual variability at all time-scales up to the length of record investigated. Major quasi-periodic oscillations, such as the QBO (Quasi-biennial Oscillation) and the 2–7 year ENSO (El Niño–Southern Oscillation) cycle have been identified in surface temperature records (Ghil and Vautard, 1991; Elsner and Tsonis, 1991) and in proxy climate data (Cole *et al.*, 1993). Such quasi-periodic cycles characterizing atmospheric flows are, however, superimposed on an appreciable 'background noise' formed by a continuum of eddies (Lorenz, 1990; Tsonis and Elsner, 1990). It is therefore important to identify the physics of multiple-scale interactions (Barnett, 1991) and to quantify the total pattern of fluctuations of atmospheric flows for predictability studies.

Deterministic chaos in computer realizations of traditional non-linear mathematical models of atmospheric flows imposes a limit on realistic simulation of flow dynamics and prediction. Selvam (1993b) has shown that round-off errors in finite precision numerical computations approximately double for every iteration. Such round-off errors enter the mainstream computation and give unrealistic solutions in long-term numerical integration schemes, such as that used in numerical weather prediction and climate models which incorporate several thousands of iterative computations.

In this paper, recently developed non-deterministic cell-dynamical-system-model (Mary Selvam, 1990, 1993a; Mary Selvam *et al.*, 1992) concepts are applied to show that the temporal (years) fluctuations of surface (air and sea) temperatures self-organize to form a universal spectrum. Such a concept rules out linear secular trends in surface temperatures.

CELL DYNAMICAL SYSTEM MODEL

In summary (Mary Selvam 1990, 1993a; Mary Selvam *et al.*, 1992) the model is based on the concepts of Townsend (1956) that atmospheric large eddy circulations form by spatial integration of enclosed turbulent

CCC 0899-8418/95/060613-11

eddies. The energy (kinetic) of successively larger eddy circulations therefore follow the statistical normal distribution characteristics according to the Central Limit Theorem. Therefore, the square of the eddy amplitude represents the eddy probability density. Such a condition, that the additive amplitudes of eddies when squared represent the probability densities, governs the subatomic dynamics of quantum systems. Atmospheric flows therefore follow quantum-like mechanical laws.

The root mean square (r.m.s.) circulation speed W of a large eddy of radius R is expressed in terms of an enclosed dominant turbulent eddy of radius r and r.m.s. circulation speed w_* as

$$W^2 = \frac{2}{\pi}\frac{r}{R} w_*^2 \tag{1}$$

The model also predicts the logarithmic wind profile relationship for atmospheric flows. The overall envelope of the large eddy traces a logarithmic spiral with the Fibonacci winding number and the quasi-periodic Penrose tiling pattern for the internal structure. Atmospheric circulation structure therefore consists of a nested continuum of vortex roll circulations (vortices within vortices) with a two-way ordered energy flow between the larger and smaller scales (equation 1).

Conventional power spectrum anlaysis of such circulation structure will reveal a continuum of eddies with progressive increase in phase.

The increase in phase $d\Theta$ as the radius R of the spiral increases from R to $R + r$ is equal to r/R. The increase in phase $d\Theta$ is therefore directly proportional to the variance W^2 (equation (1)), i.e.

$$d\Theta \propto W^2 \tag{2}$$

The phase spectrum will therefore represent the variance spectrum.

The eddy continuum has embedded dominant periodicities P_n equal to

$$P_n = \Gamma^n (2 + \Gamma) T \tag{3}$$

where Γ is the golden mean equal to $(1 + \sqrt{5})/2 = 1{\cdot}618$ and n ranges from negative to positive integer values including zero. Variable T is the primary perturbation time period equal to the annual (summer to winter) cycle of solar heating in this study of interannual variability.

Incidentally, the golden mean is associated with self-similar fractal structures generic to natural phenomana (Jean, 1992a, b; Srinivasan, 1992; Stewart, 1992). The self-similar fractal geometry of atmospheric flow structure has been documented and discussed by Tessier *et al.* (1993).

The conventional power spectrum plotted as the percentage contribution to total variance versus the logarithm of wavelength (period) will now represent the eddy probability density versus the standard deviation of the eddy fluctuations as explained in the following. The logarithm of the eddy wavelength (period) represents the standard deviation, i.e. r.m.s. value of eddy fluctuations. This follows from the concept of the logarithmic wind profile and also that the r.m.s. value of eddy fluctuations at each stage forms the mean level for the next stage of eddy growth. The r.m.s. value of the eddy fluctuations (standard deviation) can be represented in terms of the statistical normal distribution as follows. A normalized standard deviation $t = 0$ corresponds to a cumulative percentage probality density equal to 50 for the mean value of the distribution. Because the logarithm of the wavelength (period) represents the r.m.s. value of eddy fluctuations, the normalized standard deviation t is defined for the eddy energy spectrum as

$$t = (\log L / \log T_{50}) - 1 \tag{4}$$

where L is the period in years, and T_{50} is the period up to which the cumulative percentage contribution to total variance is equal to 50 and $t = 0$. Log T_{50} also represents the mean value for the r.m.s. eddy fluctuations and is consistent with the concept of the mean level represented by r.m.s. eddy fluctuations.

In the following section it is shown that continuous periodogram analyses (Jenkinson, 1977) of seasonal (September–November) mean surface (air and sea) temperature for the 28-year period (1961–1988) show that the power (variance) spectra of interannual variability follow the universal inverse power law form of the statistical normal distribution.

Further it is shown that the phase spectra represent the variance spectra as derived in equation (2).

DATA AND ANALYSIS

The seasonal (September–November) mean surface air temperature and sea-surface temperature for available grid points, numbering 1716 and 1641 respectively for the 28-year period 1961–1988, were taken from the Comprehensive Ocean Atmosphere Data Set (COADS, 1985). Figures 1 and 2 show, respectively, for surface air temperature and sea-surface temperature the location of grid-points for which unbroken data is available for the period under study.

The broadband power spectrum of the surface temperature time series can be computed accurately by an elementary but very powerful method of analysis developed by Jenkinson (1977), which provides a quasi-continuous form of the classical periodogram allowing systematic allocation of the total variance and degrees of freedom of the data series to logarithmically spaced elements of the frequency range (0·5, 0). The periodogram is constructed for a fixed set of 10 000(m) periodicities, which increase geometrically as $L_m = 2\exp(Cm)$ where C = 0·001 and $m = 0, 1, 2 \ldots, m$. The data series Y_t for the N data points was used. The periodogram estimates the set of $A_m\cos(2\pi v_m t - \phi_m)$, where A_m, v_m, and ϕ_m denote respectively the amplitude, frequency, and phase angle for the mth periodicity. The cumulative percentage contribution to total variance and the cumulative normalized (normalized with respect to the total rotation) percentage angular rotation of phase were computed starting from the high frequency side of the spectrum. The period T_{50} at which 50 per cent contribution to total variance occurs was taken as reference and the normalized standard deviation t_m values were computed as in equation (4).

$$t_m = (\log L_m/\log T_{50}) - 1$$

The cumulative percentage contribution to total variance, the cumulative normalized percentage phase rotation, and the corresponding t-values were computed for surface air temperature and sea-surface temperature respectively for all the grid-points (Figures 1 and 2) for the 28-year period 1961–1988.

The variance spectrum and the normalized phase spectrum were found to closely follow each other and also the statistical normal distribution. The 'goodness of fit' with each other and each with the normal distribution at the 95 per cent confidence level was tested using the standard statistical χ^2 test (Spiegel, 1961). Almost all the variance and a majority of phase spectra follow normal distribution characteristics.

Sets of 26 grid-points contained within approximately 10° latitude and longitude boxes were grouped together and the mean variance and phase spectra were computed for the Northern Hemisphere; shown in Figures 3 and 4 and Figures 5 and 6, respectively, for surface air temperature and sea-surface temperature. The mean variance and phase spectra for surface air and sea-surface temperatures for the Southern Hemisphere are shown in Figure 7. The cumulative normal probability density distribution is also shown in Figures 3–7. Tables I and II give the location of 10°-wide boxes and the number of grid-points in each 10° box for surface air temperature and sea-surface temperature respectively for the Northern Hemisphere. The corresponding details for the Southern Hemisphere are given in Table III.

Table IV summarizes for the Northern and Southern Hemispheres, in terms of percentages of the total number of grid-points, the following details of data and results of continuous periodogram spectral analyses for surface (air and sea) temperatures: (i) the total number of grid-points for which unbroken data is available; (ii) time-series data, which follow normal distribution characteristics; (iii) variance and phase spectra, which follow normal distribution characteristics; (iv) spectra for which T_{50} is less than 5·5 years, T_{50} being the period up to which the cumulative percentage contribution to total variance is equal to 50; (v) spectra that exhibit dominant (normalized variance > 1) periodicities in the wave bands, 2–3, 3–4, 4–8, 8–12, 12–20, and 20–48 years. The above period ranges were chosen with reference to model-predicted intrinsic periodicities of 2·2, 3·6, 5·8, 9·5, 15·3, and 24·8 years for values of n ranging from -1 to 4 (equation (3)).

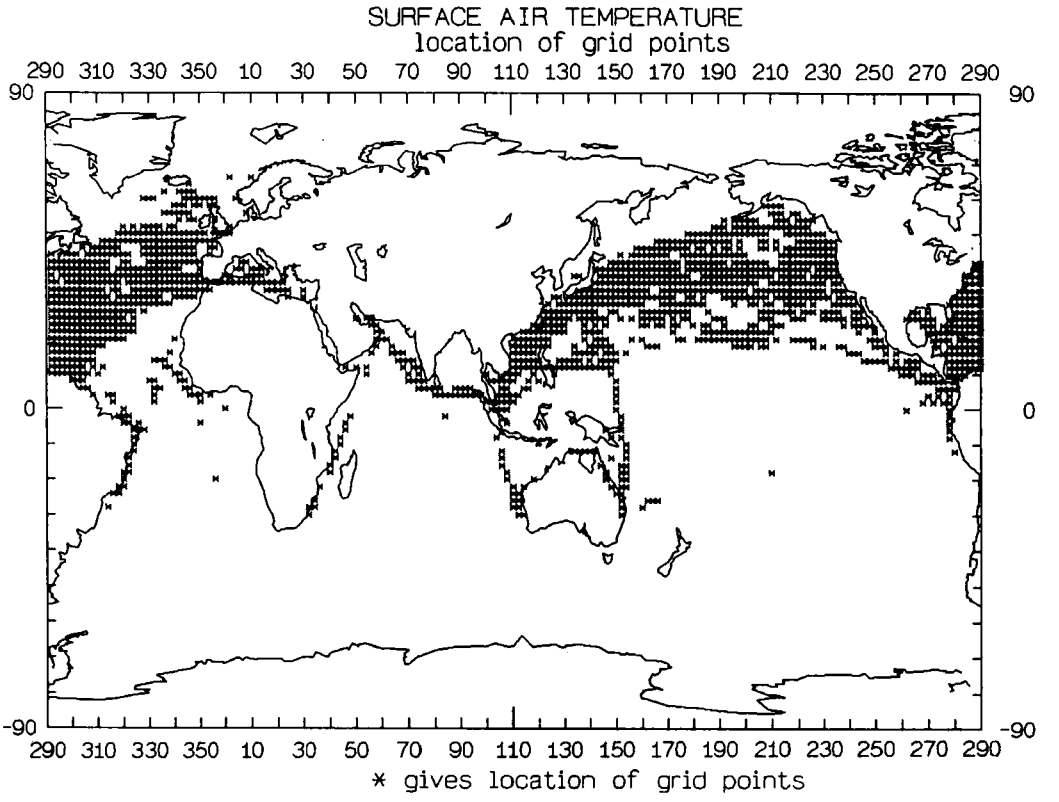

Figure 1. Location of grid-points for surface air temperature

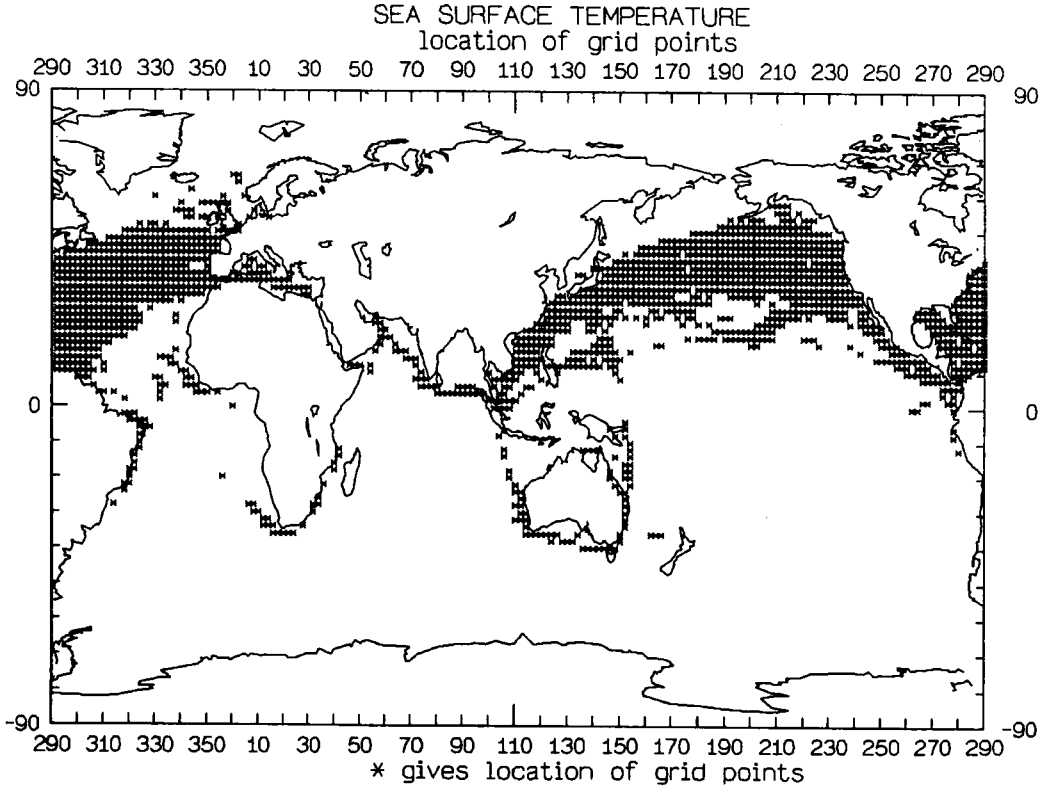

Figure 2. Location of grid-points for sea-surface temperature

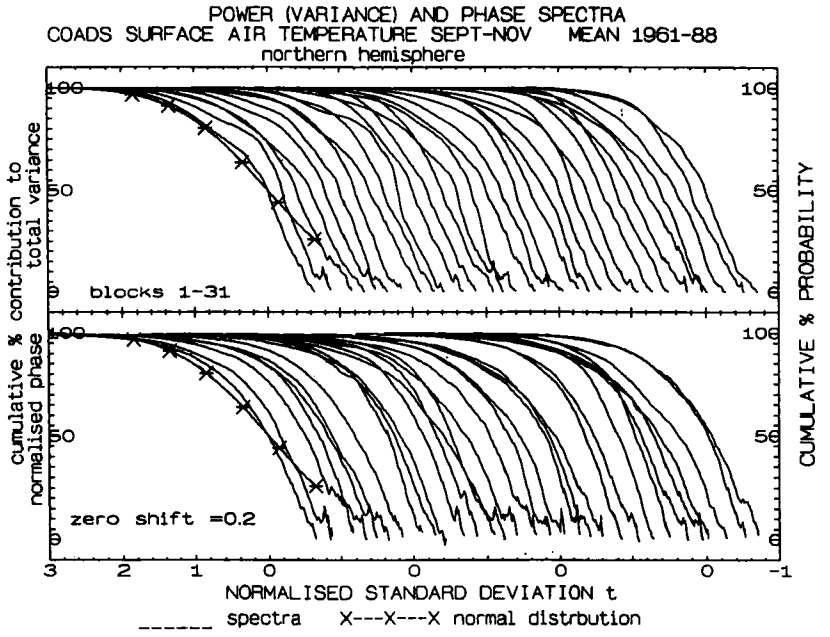

Figure 3. Mean power (variance) and phase spectra for blocks 1 to 31 listed in Table I for surface air temperature (Northern Hemisphere)

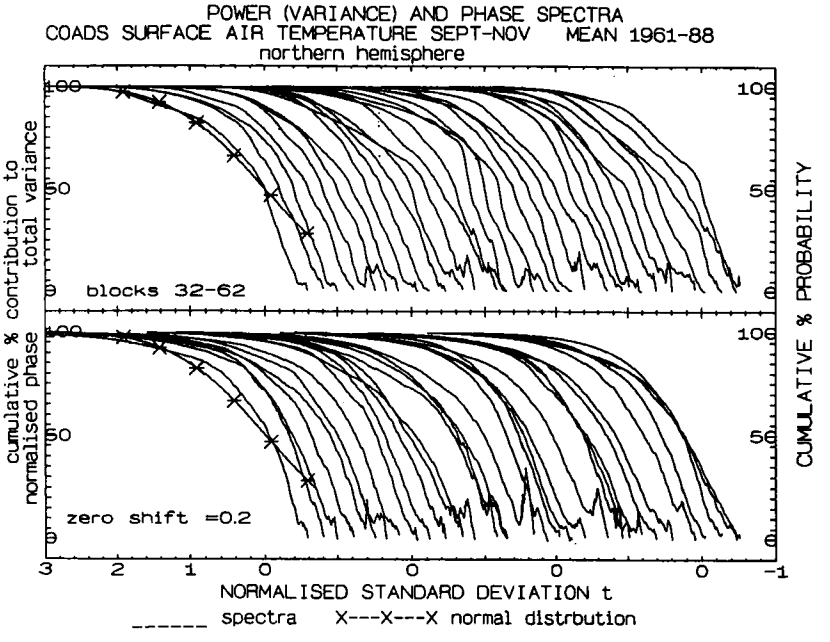

Figure 4. Same as for Figure 3 for blocks 32 to 62

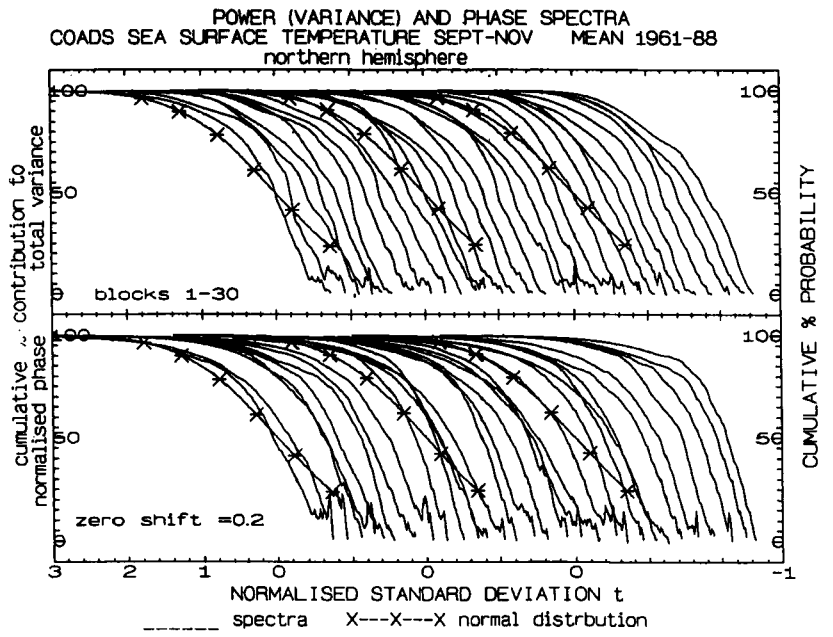

Figure 5. Mean power (variance) and phase spectra for blocks 1 to 30 listed in Table II for surface sea temperature (Northern Hemisphere)

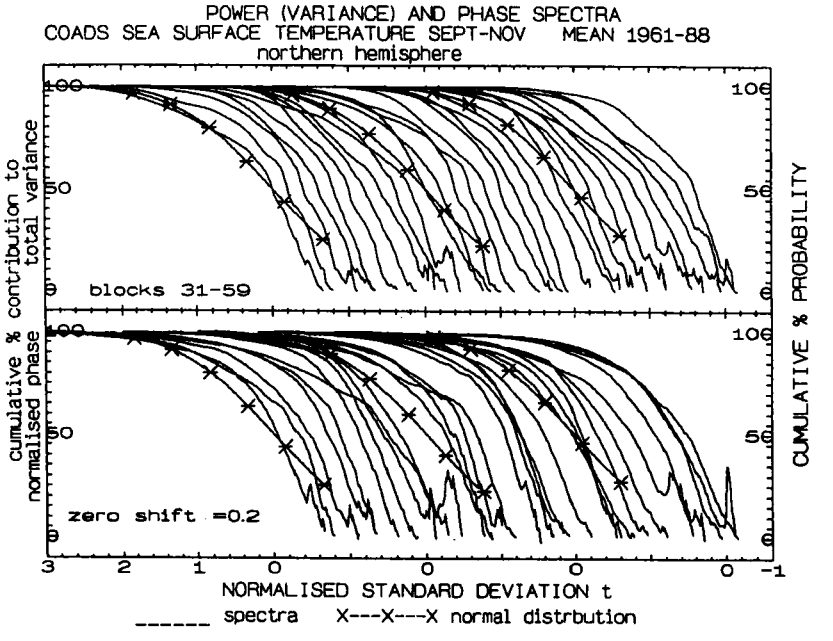

Figure 6. Same as for Figure 5 for blocks 31 to 59

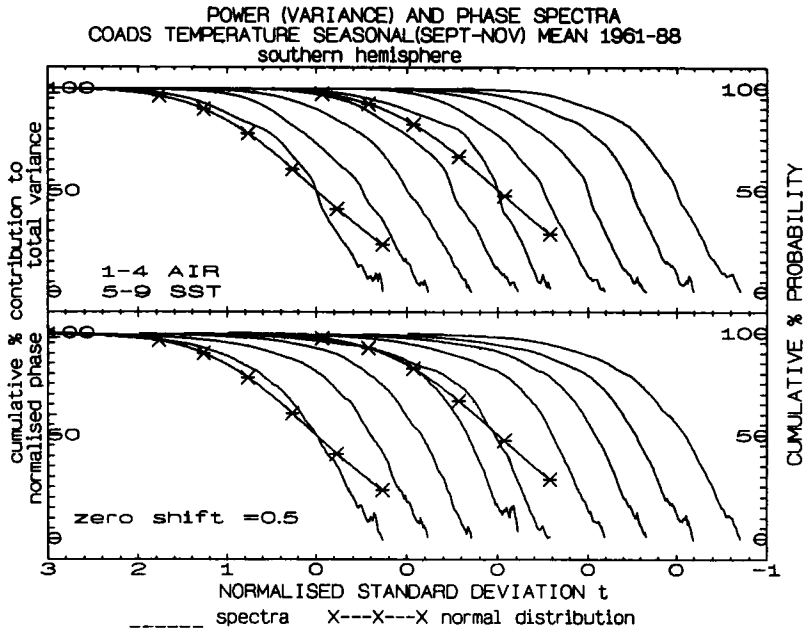

Figure 7. Mean power (variance) and phase spectra for surface air (blocks 1 to 4) and sea-surface (blocks 5 to 9) temperature listed in Table III (Southern Hemisphere)

Table I. Location of 10° blocks in the Northern Hemisphere for surface air temperature

Block number	Latitude (degrees)	Longitude (degrees)	Number of grid-points	Block number	Latitude (degrees)	Longtitude (degrees)	Number of grid-points
1	0–8	90–116	26	32	30–38	170–188	26
2	0–8	110–278	26	33	30–38	182–206	26
3	0–8	276–354	30	34	30–38	200–218	26
4	4–16	70–342	26	35	30–38	210–228	26
5	10–26	46–320	26	36	30–38	220–236	26
6	10–18	70–118	26	37	30–38	230–288	26
7	10–18	110–138	26	38	30–38	280–298	26
8	10–18	136–162	26	39	30–38	290–308	26
9	14–18	164–258	26	40	30–38	300–318	26
10	10–18	254–278	26	41	30–38	310–328	26
11	10–18	270–288	26	42	30–38	320–338	26
12	10–18	284–300	26	43	30–38	330–350	26
13	10–18	300–312	26	44	34–38	-358	26
14	20–36	20–118	26	45	40–56	-358	26
15	20–28	120–138	26	46	40–48	158–172	26
16	20–28	130–148	26	47	40–48	170–188	26
17	20–28	146–178	26	48	40–48	180–198	26
18	20–28	172–196	26	49	40–48	190–208	26
19	20–28	190–212	26	50	40–48	200–218	26
20	20–28	210–230	26	51	40–48	210–228	26
21	20–28	230–266	26	52	40–48	220–234	26
22	20–28	262–278	26	53	40–46	230–308	26
23	20–28	278–290	26	54	40–48	300–318	26
24	20–28	290–302	26	55	40–48	310–328	26
25	20–28	300–314	26	56	40–48	320–338	26
26	20–28	310–328	26	57	40–48	330–348	26
27	32–48	4–356	26	58	50–66	2–356	26
29	30–38	140–158	26	60	50–58	206–224	26
30	30–38	150–168	26	61	50–56	320–338	26
31	30–38	160–178	26	62	50–58	332–356	26

Table II.–Location of 10° blocks in the Northern Hemisphere for sea-surface temperature

Block number	Latitude (degrees)	Longitude (degrees)	Number of grid-points	Block number	Latitude (degrees)	Longtitude (degrees)	Number of grid-points
1	0–8	100–268	26	31	30–38	200–218	26
2	0–8	270–332	26	32	30–38	210–228	26
3	2–8	332–354	12	33	30–38	220–238	26
4	4–10	72–342	26	34	30–38	230–286	26
5	10–18	110–128	26	35	30–38	280–298	26
6	10–18	130–148	26	36	30–38	290–308	26
7	10–18	140–356	26	37	30–38	302–318	26
8	10–18	256–278	26	38	30–38	314–328	26
9	10–18	278–296	26	39	30–38	330–338	26
10	10–18	290–308	26	40	30–38	340–356	26
11	10–18	300–338	26	41	34–38	0–358	26
12	10–26	46–338	26	42	40–58	0–358	26
13	20–34	22–128	26	43	40–48	150–168	26
14	20–28	120–148	26	44	40–48	162–178	26
15	20–28	130–168	26	45	40–48	178–188	26
16	20–28	160–192	26	46	40–48	190–200	26
17	20–28	190–208	26	47	40–48	200–212	26
18	20–28	210–236	26	48	40–48	210–224	26
19	20–28	232–268	26	49	40–48	220–234	26
20	20–28	270–288	26	50	40–46	230–304	26
21	20–28	282–298	26	51	40–48	300–318	26
22	20–28	290–308	26	52	40–48	310–328	26
23	20–28	300–318	26	53	40–48	320–338	26
24	20–28	310–328	26	54	40–48	330–348	26
25	30–40	12–148	26	55	40–48	4–356	26
26	30–38	140–158	26	56	50–66	0–356	26
27	30–38	150–168	26	57	50–58	200–214	26
28	30–38	160–178	26	58	50–54	210–328	26
29	30–38	170–188	26	59	50–58	328–356	26
30	30–38	180–206	26				

Table III. Location of 10° blocks in the Southern Hemisphere for surface air temperature and sea-surface temperature

Surface air temperature				Sea-surface temperature			
Block number	Latitude (degrees)	Longitude (degrees)	Number of grid-points	Block number	Latitude (degrees)	Longtitude (degrees)	Number of grid-points
1	2–10	44–322	22	1	2–10	104–322	14
2	4–20	40–350	26	2	4–20	40–328	26
3	12–30	32–356	26	3	12–30	32–356	26
4	22–30	110–320	26	4	22–38	6–320	26
				5	32–40	12–166	29

Table IV. Result of (percentages of total number of grid-points) of periodogram estimate

	Parameter/ Number of grid-points	Data follow normal distri-bution	Variance spectra follow distri-bution	Phase spectra same as variance spectra	Spectra with $T_{50} \leqslant 5$ years spectra	Spectra with dominant peak periodicities (years) in the range					
						2–3	3–4	4–8	8–12	12–20	20–28
Northern Hemisphere	AIR/1616	92	90	78	76	96	74	88	50	39	15
	SST/1520	95	91	73	74	95	77	90	50	39	23
Southern Hemisphere	AIR/100	94	87	63	49	97	77	84	37	62	8
	SST/121	94	90	85	80	95	79	95	36	51	9

DISCUSSION AND CONCLUSION

From Figures 3–7 and Table IV it is seen that the variance and phase spectra of temporal (years) fluctuations of surface (air and sea) temperature follow the universal and unique inverse power law form of the statistical normal distribution, such that the square of the eddy amplitude represents the eddy probability density corresponding to the normalized standard deviation t (equation (4)). Consistent with model predictions (equations (1) and (2)), phase spectra follow closely the variance spectra (Figures 3–7).

Inverse power law for the power spectra of temporal fluctuations is a signature of self-organized criticality (Bak *et al.*, 1988) in the non-linear variability of surface temperature (air and sea). The unique quantification for self-organized criticality in terms of the statistical normal distribution presented in this paper implies predictability of the total pattern of fluctuations in the atmospheric surface temperature over a period of time, i.e. 28-years in the present study. It may therefore be possible to predict future trends in atmospheric surface temperature. The spiral-like structure predicted for the atmospheric eddy continuum is seen in the continuous smooth ordered increase of phase angle with increase in period length in the phase spectra (Figures 3–7).

The spectra exhibit dominant periodicities (Table IV) which corresponds to the model-predicted time periods of the internal circulations of the quasi-periodic Penrose tiling pattern equal to 2·2, 3·6, 5·8, 9·5, 15·3, and 24·8 years (equation (3)). Periodicities of 2–3 years and 3–7 years have been widely documented in meteorological time-series data (Lamb, 1978) and refer respectively to the high- and low-frequency components of the El Niño–Southern Oscillation (ENSO) cycle. The dominant periodicities in the atmospheric surface temperature time-series may therefore be expressed as functions of the golden mean, and these periodicities are intrinsic to atmospheric flows powered by the annual cycle of solar heating.

The dominant periodicities identified in the present study are consistent with those reported by others, as summarized in the following. Cross-spectral analysis of a 96-year oxygen isotope $\delta^{18}O$ record from a Tarawa Atoll coral (Cole *et al.*, 1993) shows a consistent and significant coherence with instrumental ENSO indices over periods centred at 2·3, 3·0, 3·6, and 5·8 years. At these periods, 75–85 per cent of $\delta^{18}O$ variance correlates linearly to ENSO. ENSO-related climate variables are characterized by broad concentrations of variance across annual, biennial, and low frequency (3–7 year) periods (Meehl, 1987; Kutsuwada, 1988; Rasmusson *et al.*, 1993). The above periods, which characterize ENSO variability, emerge in records of East Africa rainfall (Rodhe and Virji, 1976). Decadal-scale periodicities have been documented in climate data (O'Brien and Currie, 1993, and references therein).

Most of the spectra show (Table IV) that periodicities up to 5·5 years contribute to as much as 50 per cent of the total variance and therefore near-future flow-pattern trends may be estimated by high frequency periodicities up to 5·5 years.

The present study shows that atmospheric flows self-organize to form a universal eddy continuum. Such a concept rules out linear secular trends in surface (air and sea) temperatures. Warming signals may not be detectable in the near future in the presence of bidecadal and other oscillatory modes in surface air temperature (Ghil and Vautard, 1991; Tanimoto *et al.*, 1993). Greenhouse-gas-related thermal energy input into the atmospheric eddy continuum (equation (1)) may be immediately perceptible as an intensification of high-frequency components, i.e. the ENSO cycle in the global climiate.

ACKNOWLEDGEMENTS

The authors express their gratitude to Dr. A. S. R. Murty for his keen interest and encouragement during the course of this study. Thanks are due to Mr. M. I. R. Tinmaker for typing the manuscript.

REFERENCES

Bak, P. C., Tang, C. and Wiesenfeld, K. 1988. 'Self-organized criticality', *Phys. Rev. Ser. A.*, **38**, 364–374.

Barnett, T. P. 1991. 'The interaction of multiple time scales in the tropical climate system', *J. Climate*, **4**, 267–285.

COADS, 1985. *Comprehensive Ocean Atmosphere Data Set Release 1.* NOAA-ERL, Boulder, CO.

Cole, J. E., Fairbanks, R. G. and Shen, G. T. 1993. 'Recent variability in the southern oscillation: isotopic results from a Tarawa Atoll coral', *Science*, **260**, 1790–1793.

Elsner, J. B. and Tsonis, A. A. 1991. 'Do bidecadal oscillations exist in the global temperature record?', *Nature*, **353**, 551–553.
Ghil, M. and Vautard, R. 1991. 'Interdecadal oscillaions and the warming trend in global temperature time series', *Nature*, **350**, 324–327.
Jean, R. V. 1992a. 'Nomothetical modelling of spiral symmetry in biology', in Hargittai, I. (ed.) *Fivefold Symmetry*, World Scientific, Singapore, pp. 505–528.
Jean, R. V. 1992b. 'On the origins of spiral symmetry in plants', in Hargittai, I. and Pickover, C. A. (eds) *Spiral Symmetry*, World Scientific, Singapore, pp. 323–351.
Jenkinson, A. A. 1977. *A Powerful Elementary Method of Spectral Analysis for Use with Monthly, Seasonal or Annual Meteorological Time Series*. Met. O 13, Branch Memorandum No. 57, pp. 23.
Kutsuwada, K. 1988. 'Spatial characteristics of interannual variability in wind stress over the Western North Pacific', *J. Climate*, **1**, 333–347.
Lorenz, E. N. 1990. 'Can chaos and intransitivity lead to interannual variability?', *Tellus*, **42A**, 378–389.
Mary Selvam, A. 1990. 'Deterministic chaos, fractals and quantum-like mechanics in atmospheric flows', *Can. J. Phys.*, **68**, 831–841.
Mary Selvam, A. 1993a. 'A universal spectrum for interannual variability of monsoon rainfall over India', *Adv. Atmos. Sci.*, **10(2)**, 221–226.
Mary Selvam, A. 1993b. 'Universal quantification for deterministic chaos in dynamical systems', *Appl. Math. Model.*, **17**, 642–649.
Mary Selvam, A., Pethkar, J. S. and Kulkarni, M. K. 1992. 'Signatures of a universal spectrum for atmospheric interannual variability in rainfall time series over the Indian region', *Int. J. Climatol.*, **12**, 137–152.
O'Brien, D. P. and Currie, R. G. 1993. 'Observations of the 18·6 year cycle of air pressure and a theoretical model to explain certain aspects of this signal', *Climate Dyn.*, **8**, 287–298.
Rasmusson, E. M., Wang, X. and Ropelewski, C. F. 1990. 'The biennial component of ENSO variability', *J. Mar. Systems*, **1**, 71–96.
Rodhe, H. and Virji, H. 1976. 'Trends and periodicities in East African rainfall data', *Mon. Wea. Rev.*, **104**, 307–315.
Ropelewski, C. F., Halpert, M. S. and Wang, X. 1992. 'Observed tropospheric biennial variability and its relationship to the southern oscillations', *J. Climate*, **5**, 594–614.
Spiegel, M. R. 1961. *Statistics*, McGraw-Hill, New York, 359 pp.
Stewart, I. 1992. 'Where do nature's patterns come from?', *Nature*, **1835**, 14.
Srinivasan, T. P. 1992. 'Fibonacci sequence, golden ratio, and a network of resistors', *Am. J. Phys.*, **60**(5), 461–462.
Tanimoto, Y., Iwasaka, N., Hanawa, K. and Toba, Y. 1993. 'Characteristic variations of sea surface temperature with multiple time scales in the North Pacific', *J. Climate*, **6**, 1153–1160.
Tessier, Y., Lovejoy, S. and Schertzer, D. 1993. 'Universal multifractals: theory and observations for rain and clouds', *J. Appl. Meteorol.* **32**(2), 223–250.
Townsend, A. A. 1956. *The Structure of Turbulent Shear Flow*, Cambridge University Press, London, 130 pp.
Tsonis, A. A. and Elsner, J. B. 1990. 'Multiple attractors, fractals, basins and long-term climate dynamics', *Beitr. Phys. Atmos.*, **63**, 171–176.